

# Structural Phase Transitions of the Metal Oxide Perovskites SrTiO<sub>3</sub>, LaAlO<sub>3</sub> and LaTiO<sub>3</sub> Studied with a Screened Hybrid Functional

Fedwa El-Mellouhi,<sup>1,\*</sup> Edward N. Brothers,<sup>1,†</sup> Melissa J. Lucero,<sup>2</sup> Ireneusz W. Bulik,<sup>2</sup> and Gustavo E. Scuseria<sup>2,3,4</sup>

<sup>1</sup>*Department of Chemistry, Texas A&M at Qatar,*

*Texas A&M Engineering Building, Education City, Doha, Qatar*

<sup>2</sup>*Department of Chemistry, Rice University, Houston, Texas 77005-1892*

<sup>3</sup>*Department of Physics and Astronomy, Rice University, Houston, Texas 77005-1892*

<sup>4</sup>*Chemistry Department, Faculty of Science, King Abdulaziz University, Jeddah 21589, Saudi Arabia*

We have investigated the structural phase transitions of the transition metal oxide perovskites SrTiO<sub>3</sub>, LaAlO<sub>3</sub> and LaTiO<sub>3</sub> using the screened hybrid density functional of Heyd, Scuseria and Ernzerhof (HSE06). We show that HSE06-computed lattice parameters, octahedral tilts and rotations, as well as electronic properties, are significantly improved over semilocal functionals. We predict the crystal field splitting ( $\Delta_{CF}$ ) resulting from the structural phase transition in SrTiO<sub>3</sub> and LaAlO<sub>3</sub> to be 3 meV and 10 meV, respectively, in excellent agreement with experimental results. HSE06 identifies correctly LaTiO<sub>3</sub> in the magnetic states as a Mott insulator. Also, it predicts that the GdFeO<sub>3</sub>-type distortion in non-magnetic LaTiO<sub>3</sub> will induce a large  $\Delta_{CF}$  of 410 meV. This large crystal-field splitting associated with the large magnetic moment found in the G-type antiferromagnetic state suggest that LaTiO<sub>3</sub> has an induced orbital order, which is confirmed by the visualisation of the highest occupied orbitals. These results strongly indicate that HSE06 is capable of efficiently and accurately modeling perovskite oxides, and promises to efficiently capture the physics at their heterointerfaces.

PACS numbers: 71.15.Mb, 71.15.Ap, 77.80., 77.84.

## I. INTRODUCTION

Heterointerfaces between metal oxides like SrTiO<sub>3</sub> (STO), LaAlO<sub>3</sub> (LAO) and LaTiO<sub>3</sub> (LTO) show considerable promise as components in all-oxide electronics because they exhibit unique properties unobserved in the corresponding isolated parent compounds. In their bulk phase, SrTiO<sub>3</sub> and LaAlO<sub>3</sub> are non-magnetic wide-bandgap materials, but when assembled into superlattices, interesting properties such as high  $T_c$  superconductivity, magnetism, ferroelectricity and colossal magnetoresistance are observed. Despite recent experimental and theoretical activities, the field of oxide interfaces remains full of surprises and unsolved problems.<sup>1,2</sup>

A number of heterointerface behaviors have been explained using density functional theory (DFT), but several authors (see Refs. 3 and 4 and references therein) have shown that more elaborate methods like dynamical mean field theory<sup>5-7</sup> or GW-based approaches<sup>8</sup> are needed to successfully model interfaces of strongly correlated electronic systems and predict the direction of charge transfer. While many-body techniques in combination with DFT methods are sufficient for this task, they remain computationally demanding, particularly when it is necessary to account for the important structural relaxations and phase transitions occurring at interfaces.

Theory's predictive power can be enhanced by considering the properties of the two (or more) parent materials in the bulk phase, followed by mapping to obtain heterointerface properties.<sup>9,10</sup> To successfully model the perovskites considered herein, good band gaps and

accurate structural/geometric properties beyond reasonable lattice parameters are required. For example, the TiO<sub>6</sub> rotation and tilt angles are likely responsible for the metal-insulator transition in oxide superlattices<sup>11</sup> and necessitate accurate theoretical structures.

Controlling the octahedral rotations relies on good geometric values of TiO<sub>6</sub> and is considered by some to be the key to designing functional metal oxides.<sup>12</sup> Further, the TiO<sub>6</sub> rotation and/or tilts affect the electronic properties of both bulk metal oxides and their superlattices. For example, the degeneracy of the  $t_{2g}$  states in (LAO)<sub>5</sub>/(LTO)<sub>*n*</sub>/(LAO)<sub>5</sub> superlattices is lifted by the crystal field induced by the TiO<sub>6</sub> octahedral rotation in LaTiO<sub>3</sub> layer.<sup>13</sup> Consequently, accurate determination of crystal field splittings (CFS) induced by the phase transition in bulk metal oxides is also important to the Ti-3*d* orbital reconstruction at the heterointerfaces.<sup>14</sup>

Recently, Jalan *et al.*<sup>15</sup> found that stress also exerts a pronounced influence on the electron mobility in STO, with moderate strains resulting in a greater than 300% increased mobilities. Good theoretical estimation of strain in metal oxides is thus recommended and computational methods approaching the experimental strain are preferred. This is the case for the recent HSE06 calculations of Janotti *et al.*,<sup>16</sup> which confirmed the experimental findings and showed that strain in STO affects seriously the electronic effective masses and the conductivity.

A survey of literature (see Ref. 17 and references therein) presented in Table I below, summarizes the main semilocal and hybrid functional trends for bulk SrTiO<sub>3</sub>, a widely-used substrate for the heterointerface superlattices of interest here. Methods underestimating the

band gaps, like the Local Spin Density Approximation<sup>18</sup> (LSDA), the generalized gradient approximation functional of Perdew, Burke and Ernzerhof<sup>19,20</sup> (PBE), and the PBEsol<sup>21,22</sup> re-parameterization for solids must be avoided because they lead to an overestimation of the two-dimensional band at the heterointerfaces, and tend to overestimate the octahedral rotation angle in SrTiO<sub>3</sub>.

In addition, LSDA and PBE also fail to describe the antiferromagnetic insulating character in strongly-correlated systems

DFT+ $U$  methods can open the band gap to the experimental value by empirical tuning of the value of the Coulomb on-site ( $U$ ) and exchange ( $J$ ) interaction parameters, but at the cost of incorporating parameters that are external to theory and are material-dependent. While DFT+ $U$  can correctly describe the insulating character of LaTiO<sub>3</sub> in the ground state,<sup>28</sup> geometric issues like the rotation angle overestimation problems in STO, which originate from the parent functionals LSDA and PBE, do not improve by adding the + $U$  correction. Despite these well-known limitations, DFT+ $U$  has been the method of choice for the oxide superlattice calculations, mainly because the corrected gaps approach the experimental band gaps of SrTiO<sub>3</sub>, LaAlO<sub>3</sub> and LaTiO<sub>3</sub> bulk phases with a minimal additional cost compared to regular DFT calculations, especially for superlattices.<sup>29,30</sup>

Very important progress has been made in furthering our understanding of metal oxides superlattices using DFT+ $U$ ; however, one value of  $U$  will not produce the correct band gap for differing bulk metal oxides, which poses a problem for heterostructure systems like LAO/STO, LTO/STO, LTO/LAO, etc.

In fact, most DFT+ $U$  calculations assume that the value of  $U$  appropriate for the substrate is also valid to describe the grown material, as well as the heterointerface,<sup>11,28,31</sup> although in some instances the  $U$  correction is applied to the bulk only, while the grown material is treated at the regular DFT level.<sup>32</sup> (Even more sophisticated methods use different values of  $U$  and  $J$  for the Ti-3d and La-4f states; see for example Ref. 33). Another problem recently gaining notoriety is the fact that DFT+ $U$  predicts exaggerated octahedral distortions in the fully-relaxed superlattices,<sup>33</sup> which seriously affects the electronic structure and the properties of the 2-D electron gas at the interfaces. All of these shortcomings indicate the need for a universally applicable functional to better describe the electronic structure of thin films and their interfaces.

Electronic structure calculations on bulk SrTiO<sub>3</sub> using the global hybrid functionals B3PW,<sup>34</sup> B3LYP,<sup>35,36</sup> and B1-WC<sup>37</sup> were performed by several groups,<sup>24,25,38</sup> showing improved band gaps compared to semilocal DFT. For example, band gap deviations from experiment were only 6-7% with B3PW, while structural properties and order parameters of the antiferrodistortive (AFD) phase (see Table I) were also closer to experiment. Nevertheless, the use of global hybrids in studying heterointerfaces remains limited due to their high computational cost.

Screened hybrid density functionals like that of Heyd, Scuseria, and Ernzerhof<sup>39,40</sup> (HSE/HSE06) and the middle-range screened hybrid functional of Henderson, Izmaylov, Scuseria and Savin (HISS)<sup>41</sup> are excellent candidates for this task due to their accuracy and much lower computational cost compared to regular hybrids.<sup>42-45</sup> Screened hybrid functionals yield SrTiO<sub>3</sub> structural properties for both phases<sup>17,46</sup> in very good agreement with experiment,<sup>47</sup> especially if used with large (but still computationally tractable) basis sets. The best results arise from the HSE/TZVP combination.<sup>17</sup>

Previous calculations on iron<sup>48</sup> and transition metal monoxides<sup>49</sup> using HSE03<sup>50</sup> indicate that the magnetic moment, exchange splitting and band width in metals are overestimated relative to experiment. Subsequent tests on strongly-correlated magnetic materials have been carried out by Rivero *et al.*<sup>23</sup> using the short-range screened hybrid HSE06 and the long-range screened hybrid LC- $\omega$ PBE.<sup>51</sup> They demonstrated that both range-separated hybrids give a good quantitative description of the electronic structure of strongly-correlated systems, with magnetic coupling constants that are larger than experiment, yet improved compared to the results of the global hybrid, B3LYP.

A more recent work from Philipps and Peralta<sup>52</sup> involving transition metal molecular complexes suggests that HSE06 is a promising alternative for the evaluation of exchange couplings in extended systems, again because of reasonable accuracy at reduced computational expense. The present paper is a continuation of earlier work<sup>17</sup> with SrTiO<sub>3</sub>: herein, we assess the accuracy of HSE06 for calculating the crystal field splitting in SrTiO<sub>3</sub>, the geometries of LaAlO<sub>3</sub> in its different phases, as well as the structural and magnetic properties of the strongly-correlated system, LaTiO<sub>3</sub>.

## II. COMPUTATIONAL METHODS

All calculations presented in this paper were performed using a development version of the GAUSSIAN suite of programs,<sup>53</sup> with the periodic boundary condition (PBC)<sup>54</sup> code used throughout. Unless otherwise noted, crystal structures were downloaded as CIF files from the ICSD.<sup>55</sup> (See Ref. 55 for the specific ID numbers.)

The Def2-<sup>56</sup> series of Gaussian basis sets were optimized for use in bulk LaTiO<sub>3</sub> and LaAlO<sub>3</sub> calculations, following the procedure described in Ref. 17 for bulk SrTiO<sub>3</sub>. We use the notation TZVP and SZVP to differentiate these optimized PBC basis sets from the molecular Def2-TZVP and Def2-SZVP basis sets. The functionals applied in this work include the LSDA<sup>18</sup> (SVWN5),<sup>57</sup> PBE, and HSE06. LSDA and PBE calculations were utilized to assess the quality of the Gaussian basis sets via comparison with planewave calculations from the literature.

Most numerical settings in GAUSSIAN were left at the

TABLE I. Trends observed in the performance of DFT and post-DFT calculations applied to bulk SrTiO<sub>3</sub> regardless of the basis sets used (see Ref. 17). Hybrids account for both global (B3PW,<sup>24-26</sup> B3LYP<sup>26</sup> and B1-WC.<sup>27</sup>) and screened (HSE and HISS) hybrid functionals.

Functional	LSDA	PBEsol	PBE	DFT+U	Hybrids
Lattice parameter	Too Low	Good	Too Big	Too Low	Good
Band gaps	Too Small -40%	Too Small -40%	Too Small -40%	Good	Good ±6%
TiO <sub>6</sub> rotation angle	Too Big Up to 8°	Too Big 5°	Too Big 4°	Too Big 4-5°	Good 1-2°

default values, *e.g.*, geometry optimization settings, integral cut-offs, *k*-point meshes and SCF convergence thresholds. For LaAlO<sub>3</sub>, the reciprocal space integration used a 12×12×12 *k*-point mesh for the cubic unit cells of 5 atoms, while for the larger rhombohedral supercell of 30 atoms, the default *k*-point mesh of 8×8×4 was found to be sufficient. Because we performed optimizations of both atomic positions and lattice parameters, the SCF convergence threshold was set to TIGHT, or 10<sup>-8</sup> atomic units. The fully relaxed structures can be obtained from the Cambridge Structural Database.<sup>58</sup>

Due to the metallic nature of LaTiO<sub>3</sub>, a mesh of 24×24×18 for the *k*-point sampling was required in order to ensure stable convergence.<sup>48</sup> For the sake of computational efficiency, all calculations on LTO were carried out using the SZVP basis set.

### III. RESULTS AND DISCUSSION

#### A. SrTiO<sub>3</sub>

Under ambient conditions, bulk SrTiO<sub>3</sub> crystallizes in a cubic perovskite structure, subsequently undergoing a second order phase transition at  $T_c=105$  K to a tetragonal structure with slightly rotated oxygens around the *z*-axis, known as the antiferrodistortive (AFD) phase. The phase transition of STO is governed by two order parameters. The primary order parameter is the rotation angle of the TiO<sub>6</sub> octahedra ( $\theta$ ) that can reach up to 2.1° at 4.2 K.<sup>59</sup> The second order parameter measures the tetragonality of the unit cell, as defined by the ratio of *c/a*, and can be as large as 1.0009 upon cooling to 10 K.<sup>60</sup>

The finer details of the conduction band splitting induced by the AFD phase transition in STO are still under debate,<sup>61-64</sup> with discrepancies between theory and experiment arising from differences in the sample dopant or defect concentrations: the TiO<sub>6</sub> rotation angle may be enhanced or reduced depending on the doping conditions and this affects directly the rotation of oxygen atoms in the *xy*-plane when STO distorts into the AFD phase.

We have shown<sup>17</sup> in modeling an idealized STO (with

no defects, doping, strain or surface effects) that HSE06 provides band gaps and phase transition order parameters in excellent agreement with experiment. We found a  $c/a=1.0012$  corresponding to a +0.12% tensile strain along the [001] direction or the *z*-axis. However, we did not address the crystal field splitting ( $\Delta_{CF}$ ) of the conduction band minimum (CBM) induced by the phase transition. As is evident from the enlargement of the region around the calculated CBM at the  $\Gamma$  point the crystal field causes the 3-fold degenerate band to split into a doubly-degenerate band and a single band 3 meV higher in energy.

Further discussion arise from figure 1 by zooming at 10% from Brillouin zone center along the high symmetry directions, [100] ( $\Delta$ ), [001] ( $D$ ), [101] ( $S$ ), [110] ( $\Sigma$ ) and [111] ( $\Lambda$ ) in the body centered tetragonal Brillouin zone. Along  $\Delta$ ,  $D$ , and  $S$ , we observe a qualitative behavior very similar to that predicted in an earlier augmented plane wave (APW) calculation without spin-orbit (SO) coupling.<sup>64</sup> However, differences arise along  $\Sigma$  and  $\Lambda$  directions where we observe that the lowest doubly degenerate band splits into a heavy electron (*he*) and light electron (*le*) bands as we move farther from the  $\Gamma$  point. The differences might come from the model used in the APW calculation by Mattheiss neglecting both the nearest and second-nearest neighbor oxygen-oxygen 2*p* interactions and the interaction between the oxygen-2*s* and the titanium *t*<sub>2*g*</sub> orbitals in the cubic state.

Quantitatively, the APW calculations predict  $\Delta_{CF}^{APW}=20.7$  meV which is much greater than the  $\Delta_{CF}^{HSE06} = 3$  meV we obtain in the present work. This is also the case for the spin-orbit splitting for cubic STO  $\Delta_{SO}^{APW}=83$  meV, if compared with  $\Delta_{SO}^{HSE06}=28$  meV computed using the VASP planewave code by Janotti et *al.*<sup>16</sup>

Janotti et *al.* studied with HSE06 the effect of ±1% strain on the CBM focusing on the splittings and the electron effective masses taking into account the spin-orbit effects. They also found that the rotation of TiO<sub>6</sub> octahedra around the *z*-axis without including the tetragonal distortion ( $c > a$ ) lead to a splitting of the doubly degenerate band of 4 meV with minor changes on the effective masses. Going back to our results in figure 1, one concludes that the small +0.12% tensile strain along

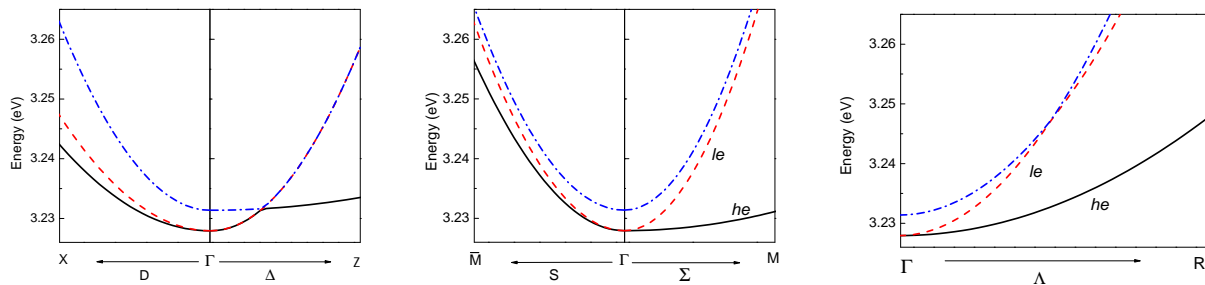


FIG. 1. (Color online) Enlargement of the region around calculated conduction band minimum (CBM) at the  $\Gamma$  point showing the splitting in  $\text{SrTiO}_3$  caused by the AFD phase transition. The high symmetry directions are those of the body centered tetragonal lattice [100] ( $D$ ), [001] ( $\Delta$ ), [101] ( $S$ ), [110] ( $\Sigma$ ), [111] ( $\Lambda$ ) and  $Z = (00\frac{1}{2})$ ,  $\bar{M} = (\frac{1}{2}0\frac{1}{2})$ .

the [001] direction arising from the tetragonal distortion might not contribute significantly to the CBM splitting but plays a role on the important differences in the electron effective masses we observe along the high symmetry directions. For example, the curvature of the CBM is higher (i.e. lower effective mass or light electrons- $le$ ) along  $S$  and  $\Delta$  directions –parallel to the strain– indicating higher electron mobilities in those directions. This result is in line with the enhanced electron mobility Janotti *et al.* concluded for  $\text{SrTiO}_3$  subject to +1% tensile strains along the (001) direction. However, further investigation is still needed to draw a final conclusion since the electron effective masses and the order of the bands change upon the inclusion of SO effects.<sup>16</sup>

The combined HSE06 results,  $\Delta_{CF}^{HSE06}$  and  $\Delta_{SO}^{HSE06}$  show an excellent *quantitative* agreement with experimental data obtained from single domain Shubnikov-de Haas oscillation Raman spectroscopy measurements,<sup>63</sup> namely:  $\Delta_{CF}^{exp} = 2$  meV and  $\Delta_{SO}^{exp} = 18$  meV. However, they do not support the picture proposed by the recent angle resolved photoemission spectroscopy (ARPES) experiment of Chang *et al.*,<sup>62</sup> which indicates that the single band is of lower energy, with a doubly-degenerate band 25 meV higher. This disagreement may arise from the fact that STO samples used in this experiment were doped with oxygen vacancies ( $V_O$ ), which are known to introduce a shallow defect level in the band gap of STO.<sup>65</sup> Finally, using HSE06 and the TZVP basis set to model STO relaxed in the AFD phase, we found that the crystal field splits the CBM at the gamma point by 3 meV, leaving it doubly degenerate in the absence of SO coupling.

## B. $\text{LaAlO}_3$

Bulk  $\text{LaAlO}_3$  undergoes a phase transition from the simple cubic structure to a rhombohedral-central hexagonal structure with space group  $R\bar{3}C$  at temperatures below 813 K.<sup>66–68</sup> The two order parameters for this phase transition are the tilt of the  $\text{AlO}_6$  octahedra ( $\Theta$ ), which can reach a maximum value of  $5.7^\circ$  at 4.2K,<sup>67</sup> and  $\tau$ , a measure of spontaneous strain, defined as  $\tau = c/a - \sqrt{6}$ ,

with values of up to -0.008. The calculated lattice parameters relative to experiment for both phases of bulk LAO are underestimated with LSDA, overestimated with PBE and in-between for HSE06 (Table II). This is well-known behavior for LSDA and PBE (see *e.g.* Ref. 69 and references therein), and has been observed in a large number of semiconducting materials, as well as in our recent study on  $\text{SrTiO}_3$ .<sup>17</sup>

In the low temperature rhombohedral phase, the LSDA and PBE lattice parameters tend to be higher than previous plane-wave calculations.<sup>71–73</sup> The octahedral tilt angle for both LSDA and PBE is ca.  $4^\circ$ , which is 30% smaller than the maximum tilts measured experimentally. The SZVP basis set produces tilt angles 30% lower than those observed by plane-wave calculations<sup>73</sup> which is very similar to the behavior we observed in the case of STO: we attribute this to the use of localized basis sets.<sup>17</sup> HSE06 yields lattice parameters for the cubic phase in excellent agreement with experiment, with a deviation of only 0.25%, and improved rhombohedral lattice parameters deviating by 0.5% compared to 1.5% with PBE. Improvement of the same magnitude was also obtained using the recently introduced variational pseudo self-interaction correction approach (VPSIC<sub>0</sub>).<sup>74</sup>

The calculated spontaneous strain ( $\tau$ ) is also significantly closer to experiment for HSE06 and LSDA than PBE. For all functionals considered here, the calculated lattice mismatch between cubic LAO and STO agree with the 2% value reported in the experiment, indicating that the basis set we used will not introduce any additional strain in LAO/STO superlattices beyond those inherently present in the experimentally measured ones.

Turning now to the electronic properties of LAO, our computed band gaps are summarized in Table III. Comparisons with experimental band gaps are relative to the room temperature rhombohedral phases since, to our knowledge, no experimental measurements of the cubic phase band gap exist.

In general, band gaps calculated using the LSDA and PBE are underestimated in average by  $\sim 30\%$  or  $\sim 1.8$  eV compared to experiment, with PBE doing better than the LSDA. This is consistent with earlier calculations<sup>71,72</sup>

TABLE II. Calculated lattice parameters of LAO as well as phase transition order parameters: the octahedral tilt angle ( $\Theta$ ) and the spontaneous strain ( $\tau = c/a - \sqrt{6}$ ). Values with a reference number come from previous experimental and/or planewave calculations.

	Rhombohedral			$\Theta(^{\circ})$	$\tau$	Cubic
	a ( $\text{\AA}$ )	b ( $\text{\AA}$ )	c ( $\text{\AA}$ )			a=b=c ( $\text{\AA}$ )
Experiment <sup>a</sup>	5.365	5.365	13.111	5.7	-0.008	3.810 <sup>b</sup>
LSDA	5.341, 5.290 <sup>e</sup>	5.339	13.020	4.1, 6.1 <sup>e</sup>	-0.012	3.760, 3.750 <sup>c</sup>
PBE	5.448, 5.370 <sup>d</sup>	5.444, 5.370 <sup>d</sup>	13.250, 13.138 <sup>d</sup>	4.0	-0.017	3.830
HSE06	5.398	5.393	13.160	3.1	-0.011	3.800

<sup>a</sup> At 4.2 K from Ref 67

<sup>b</sup> Ref 70

<sup>c</sup> Ref 71

<sup>d</sup> Ref 72

<sup>e</sup> Ref 73

TABLE III. Calculated band gaps of LaAlO<sub>3</sub> using the SZVP basis set compared to experimental values. Data from this work are listed first, followed by data from previous planewave simulations and citations.

Band gap(eV)	Rhombohedral		Cubic
	Direct	Indirect	Direct
Experiment	5.60 <sup>a</sup>	—	—
LSDA	3.75, 3.87 <sup>e</sup>	3.25, 3.3 <sup>b</sup>	3.46
PBE	3.98, 3.95 <sup>c</sup>	3.27, 3.1 <sup>f</sup>	3.54
HSE06	5.24	4.77	5.04

<sup>a</sup> Ref 75

<sup>b</sup> Ref 71

<sup>c</sup> Ref 72

<sup>d</sup> Ref 76

<sup>e</sup> Ref 73

<sup>f</sup> Ref 77

and indicates that the basis set does not negatively impact electronic structure properties in a significant manner, a behavior we observed in the STO case as well.<sup>17</sup> (Please see Table II for comparisons with previous calculations.) As expected, HSE06 provides a much better estimate of the band gaps, even when using the smaller SZVP basis sets, with deviations from experiment not exceeding 0.36 eV or 6% for the rhombohedral phase. This error is larger than the 1% deviation observed in the SrTiO<sub>3</sub> case, but is well-within the 0.3-0.4 eV range for non-ionic bulk semiconductors.<sup>42-44,78</sup>

For the cubic phase, HSE06 produces an indirect band gap of 4.7 eV, which agrees well with the calculated gap of 4.4 eV obtained using the screened exchange method<sup>77,79</sup> (sX) and planewave basis sets and the 4.61 eV gap obtained using the VPSIC<sub>0</sub> method.<sup>74</sup> The HSE06 direct gap is 5.0 eV, which lies between the VPSIC<sub>0</sub><sup>74</sup> value of 4.89 eV and the GW-corrected LSDA band gap at the experimental lattice constants<sup>76</sup> of 5.68 eV. The quality of the cubic phase results is encouraging for future heterostructure and defect state calculations because LAO films grown on Si substrates, using a few STO layers as a template, usually adopt the cubic structure.<sup>80</sup> The cubic and rhombohedral phase band structures as calcu-

lated by HSE06 for LaAlO<sub>3</sub> are shown in Figure 2. They look very different because the Brillouin zone sampling and the number of atoms in each simulation supercell are different, but as we will demonstrate with the projected densities of states (PDOS), only small changes in the spectrum occur at the phase transition.

Starting from the cubic phase, the band gap is indirect (R $\rightarrow$  $\Gamma$ ) with a doubly degenerate CBM and a triply degenerate valence band maximum, VBM. A close look at our computed CBM in the rhombohedral phase also reveals that the phase transition induces a lift of degeneracy at the CBM and a splitting at the  $\Gamma$  point with  $\Delta_{CF}=10$  meV. The band gap increase and  $\Delta_{CF}$  for LAO are much higher than the values we reported for SrTiO<sub>3</sub>; we attribute this to the fact that six of six oxygens are experiencing significant rigid octahedral tilts leading to changes in the La-O-La angles from the ideal 180 $^{\circ}$  to 173.8 $^{\circ}$ , compared to a smaller rotation resulting from a 4/6 oxygen ratio in the STO case.

By aligning the VBM of both phases (see the right of Figure 2) we observe that the octahedral tilt leads to a shift of the CBM to higher energies, thus increasing the band gap by 500 meV. There is also experimental evidence that the crystal field caused by AlO<sub>6</sub> tilts in LaAlO<sub>3</sub> induces splitting of the CBM; but no quantitative values were reported.<sup>67</sup>

By looking at the PDOS (Figure 3) we observe that the VBM is strictly dominated by O-2p states, while La-5d states dominate the CBM. Unlike the SrTiO<sub>3</sub> case, no significant intermixing between the O-2p and La-5d states is observed, indicating that the bonding has predominately ionic character. This picture is not affected by the phase transition, and no signs of orbital intermixing is observed in the rhombohedral phase PDOS as well, where peaks conserve their height and shape (not shown).

In summary, by applying HSE06 to LAO we lose some agreement with experiment on the octahedral tilts but we gain better precision than semilocal functionals in the band gaps, lattice parameters and strain altogether. In other words, overall HSE06 provides a more physically accurate picture.

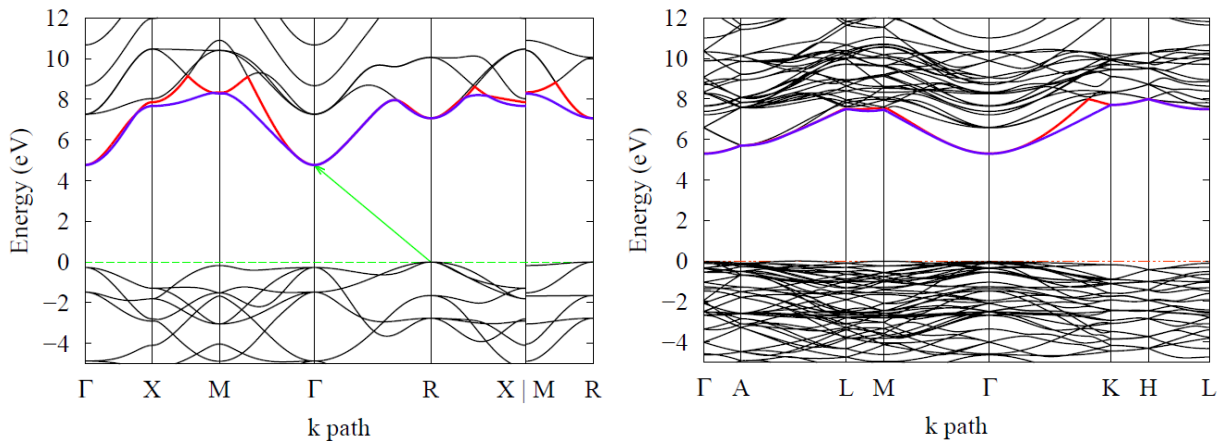


FIG. 2. (Color online) Band structure of  $\text{LaAlO}_3$  calculated using HSE06 for the high temperature cubic phase (**Left**) and the low temperature rhombohedral phase (**Right**). The dashed line depicts the Fermi level at the valence band maximum (VBM).

### C. $\text{LaTiO}_3$

$\text{LaTiO}_3$  adopts a  $Pbnm$ ,  $\text{GdFeO}_3$ -type orthorhombic structure ( $a \neq b \neq c$ ) with tilted and rotated  $\text{TiO}_6$  octahedra (see Figure 4) in the simulation supercell of 20 atoms, with no experimental evidence of a simpler cubic structure. The tolerance factor of a perovskite compound  $\text{ABO}_3$ ,  $t$ , is defined as the ratio of the intrinsic sizes of the  $\text{AO}$  square and the  $\text{BO}_2$  square:<sup>81,82</sup>

$$t = \frac{r_A + r_O}{\sqrt{2}(r_B + r_O)} \quad (1)$$

where  $r_A$ ,  $r_B$  and  $r_O$  are the ionic radii of each ion. In  $\text{LaTiO}_3$ , the tolerance factor is too small to favor the cubic structure due to the relative size of  $\text{La}^{+3}$  ion to the  $\text{TiO}_6$  octahedra.

Nevertheless, the octahedral tilts ( $\Theta$ ) stabilize the structure by shortening some La-O bonds (see Figure 4-a) and causing  $\text{Ti-O}_1\text{-Ti}$  angles to deviate from  $180^\circ$ . Any neighboring pair the  $\text{TiO}_6$  octahedra would tilt around the  $z$ -axis in opposite directions. The subsequent rotation with respect to the same axis ( $\phi$ ), is restricted to  $\text{O}_2$  oxygens forming the basal plane of the  $\text{TiO}_6$  and occur in the same sense. In addition, Cwik et al.<sup>70</sup> showed that the negative sign of their orthorhombic distortion parameter ( $\epsilon = (b - a)/(b + a)$ ) demonstrates that the  $\text{TiO}_6$  octahedra are distorted. The  $\text{TiO}_6$  basal plane is rectangular-like instead of cubic with the  $\text{O}_2\text{-O}_2$  edge lengths splitting into  $d_{\text{O}_2\text{-O}_2}^{\text{long}}$  and  $d_{\text{O}_2\text{-O}_2}^{\text{short}}$  with a ratio:

$$r_{\text{O}_2\text{-O}_2} = \frac{d_{\text{O}_2\text{-O}_2}^{\text{long}}}{d_{\text{O}_2\text{-O}_2}^{\text{short}}} \quad (2)$$

$r_{\text{O}_2\text{-O}_2}$  reaches up to 1.04 at 8 K. The octahedron's basal plane angles also deviate from the ideal  $90^\circ$  (see Figure 4-c) leading to differences in the  $\text{Ti-O}_2$  distances

namely,  $d_{\text{Ti-O}_2}^{\text{long}}$  and  $d_{\text{Ti-O}_2}^{\text{short}}$  and the ratio:

$$r_{\text{Ti-O}_2} = \frac{d_{\text{Ti-O}_2}^{\text{long}}}{d_{\text{Ti-O}_2}^{\text{short}}} \quad (3)$$

$\text{LaTiO}_3$  undergoes a phase transition from a non-magnetic insulator to an antiferromagnetic Mott insulator at temperatures near  $T_c=146$  K without undergoing important changes in the structural parameters.<sup>70</sup> To determine the initial geometry for LTO, we fully-relaxed a non-magnetic 20-atom LTO supercell with the PBE and HSE06 functionals, starting from several experimental structures acquired at different temperatures.<sup>70,83,84</sup> All structures relaxed to the same minimum. The lattice parameters of the fully-relaxed non-magnetic structure with both PBE and HSE06 are summarized in Table IV and compared to experimental data taken at  $T=155$  K just above the phase transition temperature.

Using HSE06, we observe excellent agreement with experiment as shown by the orthorhombic distortion parameter<sup>85</sup> ( $\epsilon$ ) being of the right sign and magnitude. In addition,  $r_{\text{O}_2\text{-O}_2}$  and  $r_{\text{Ti-O}_2}$  ratios compare very well with experiment<sup>70,83</sup> an indication that the octahedral distortion is well reproduced. With PBE,  $\epsilon$  has a positive sign which suggests that the  $\text{TiO}_6$  octahedra elongate along  $b$  instead of  $a$  which qualitatively incorrect. The last behavior has been reported previously in Ref. 28 as a drawback of LSDA that have been overcome by adding the adequate  $U$  correction<sup>86</sup> (See the LSDA+ $U$  results in Table IV). Also,  $r_{\text{O}_2\text{-O}_2}$  and  $r_{\text{Ti-O}_2}$  ratios indicate that  $\text{TiO}_6$  octahedra are nearly ideal and do not reproduce the distortion observed experimentally. The octahedral tilt ( $\Theta$ ) and rotation angles ( $\Phi$ ) are underestimated by 2 and  $0.45^\circ$ , respectively with HSE06, but the underestimation is worse in the PBE case, reaching 3.3 and  $2.85^\circ$ , respectively.

Turning to the electronic properties, the calculated projected density of states for  $\text{LaTiO}_3$  in the non-magnetic state (Figure 5) are similar for HSE06 and PBE

TABLE IV. Lattice constants and orthorhombic distortion parameters as well as octahedral tilt ( $\Theta$ ) and rotation angles ( $\Phi$ ) calculated using SZVP basis set for the fully-relaxed  $\text{LaTiO}_3$  structures. Comparison is done with experimental data taken at 155K from Ref. 70 near the magnetic to antiferromagnetic transition temperature  $T_N = 146$  K.

	a (Å)	b(Å)	c(Å)	$\epsilon$	$r_{O_2-O_2}$ <sup>d</sup>	$r_{Ti-O_2}$ <sup>d</sup>	$\Theta(^{\circ})$	$\Phi(^{\circ})$
Experiment <sup>a</sup>	5.635	5.602	7.905	-0.0030	1.035	1.011	12.86	9.69
HSE06	5.600	5.534	7.904	-0.0059	1.027	1.013	10.88	9.25
PBE	5.595	5.632	7.938	+0.0033	1.008	0.998	9.54	6.85
LSDA <sup>b</sup>	5.462	5.524	7.789	+0.0056	—	—	—	—
LSDA+ $U$ <sup>c</sup>	5.586	5.529	7.89	-0.0051	—	—	—	—

<sup>a</sup> At 155K from Ref. 70

<sup>b</sup> Ref 28

<sup>c</sup> For the optimum values of  $U=3.2$  and  $J=0.9$  eV identified in Ref. 28

<sup>d</sup> Distances evaluated for the same set of reference atoms.

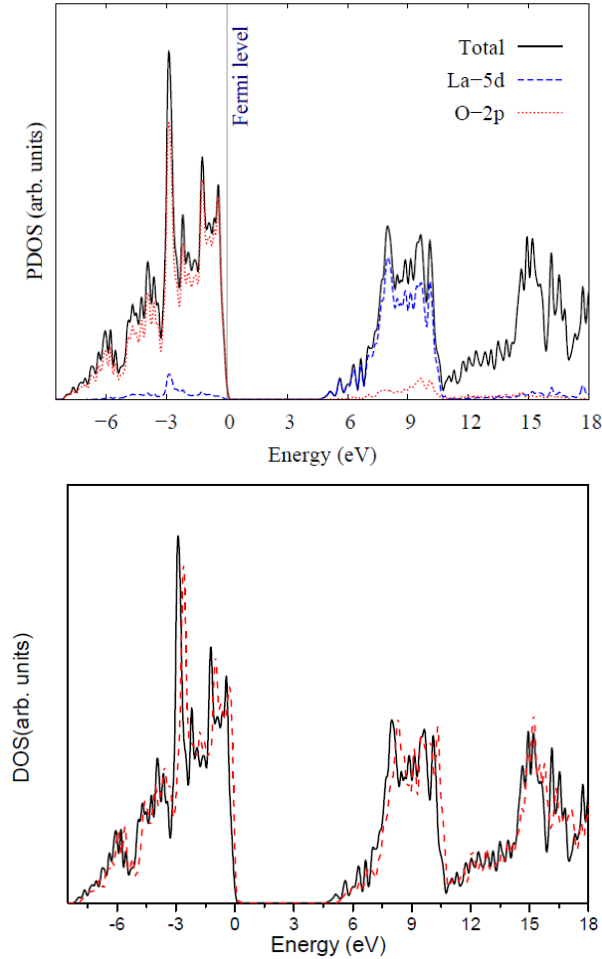


FIG. 3. (Color online) **Top:** Projected electronic densities of states (PDOS) for  $\text{LaAlO}_3$  calculated using HSE06 in the cubic phase. **Bottom:** Changes in the total density of states upon the phase transition from cubic (solid line) to rhombohedral (dashed line) mainly characterized by a shift of the conduction band states to higher energies.

showing metallic behavior and a Fermi level lying at the middle of the  $\text{Ti-3d}$  band.<sup>87</sup> The  $\text{Ti-3d}$  band is separated

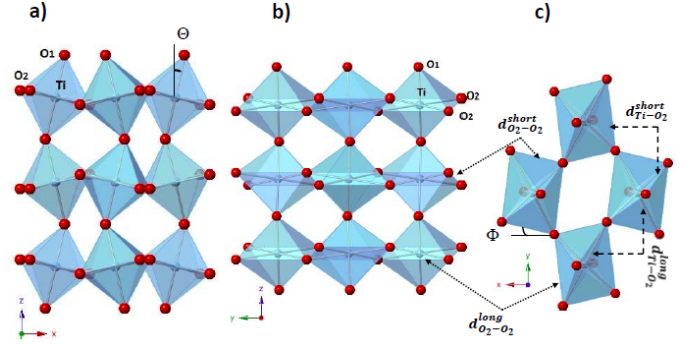


FIG. 4. (Color online) Tilted and rotated  $\text{TiO}_6$  octahedra in  $\text{LaTiO}_3$  viewed along: **a)** 010 direction showing the octahedral tilts ( $\Theta$ ) with respect to the  $z$ -axis **b)** 100 direction featuring the rectangular-like basal plane of the  $\text{TiO}_6$  octahedra and **c)** 001 direction showing clearly the octahedral rotation ( $\Phi$ ), the orthorhombic distortion and the different interatomic distances arising from it. Note that the lattice parameters  $b$  have been increased by 35% for a better illustration of basal plane distortion.

from the  $\text{O-2p}$  band by 3.95 and 2.87 eV for HSE06 and PBE, respectively. As with  $\text{SrTiO}_3$ , the valence band (VB) is dominated by  $\text{O-2p}$  states while the conduction band is dominated by  $\text{Ti-3d}$  states with some intermixing between  $\text{O-2p}$  and  $\text{Ti-3d}$  orbitals, indicating a partially covalent bond.

The band structure in the bottom of figure 5 show more details about the  $\text{O-2p}$  and  $\text{Ti-3d}$  band separation where the  $t_{2g}$  triplet states<sup>88,89</sup> can be distinguished by their colors. The  $\text{GdFeO}_3$ -type distortion causes a large crystal field splittings ( $\Delta_{CF}$ ) defined as the separation between the two first  $t_{2g}$  triplet states<sup>88,89</sup> at the  $\Gamma$  point and a subsequent smaller splitting ( $\Delta'_{CF}$ ) between the second and the third states. The amount of  $\Delta_{CF}$  is strongly correlated to the orbital state of LTO (see the review paper of Mochizuki and Imada<sup>90</sup> and the recent paper of Krivenko<sup>89</sup>) with small CFS inducing orbital liquid state (OL),<sup>86,91</sup> while large CFS favoring an induced orbital ordering (IO).<sup>74,92-94</sup>

With HSE06,  $\Delta_{CF}$  is about 410 meV, somewhat larger

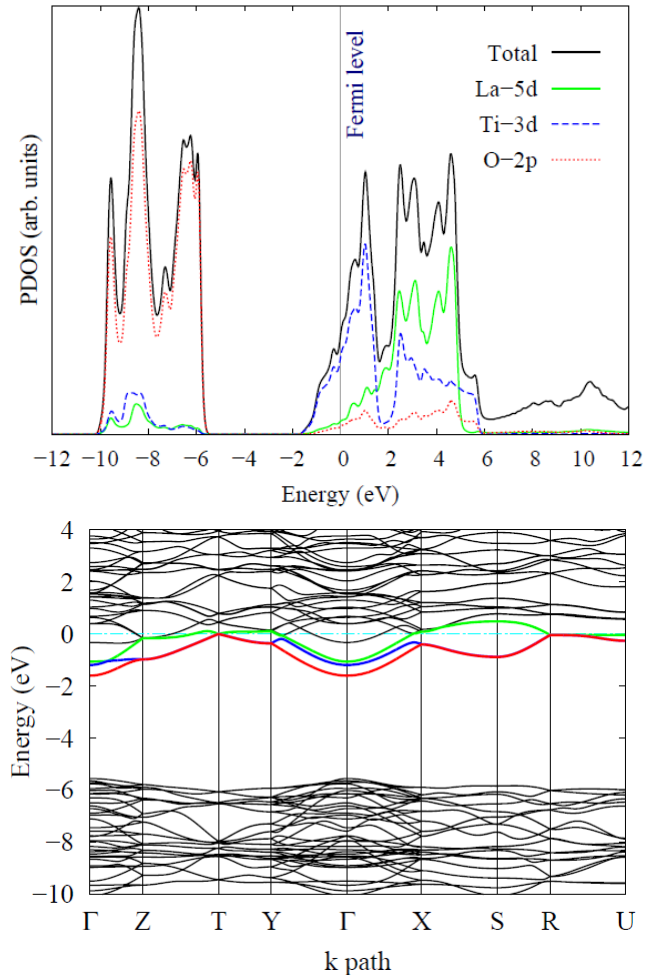


FIG. 5. (Color online) **Top:** Total and projected density of states for orthorhombic  $\text{LaTiO}_3$  as calculated with HSE06 and the SZVP basis set. Only the contribution from the dominant states are represented. **Bottom:** The corresponding band structure of  $\text{LaTiO}_3$  in the non-magnetic state. The Ti  $t_{2g}$  triplet bands can be distinguished by their colors where the splittings caused by octahedral deformation can be clearly seen.

than the experimental splittings of 240 meV<sup>70</sup> and 300 meV<sup>92</sup> evaluated for non magnetic solutions. With PBE, we find a much smaller  $\Delta_{CF}$  of 61 meV, which is consistent with LSDA+ $U$  calculations ranging between 37-54 meV.<sup>91,95</sup> This small CFS is a shared feature between semilocal functionals and might be at the origin of the unsettled theoretical description of the orbital state of bulk  $\text{LaTiO}_3$ .<sup>89,90</sup> With HSE06,  $\Delta'_{CF} = 190$  meV which is high compared to the nearly degenerate doublet observed experimentally.<sup>70</sup> This difference probably comes from the higher orthorhombic distortion we observe in our defect-free relaxed structures which is known experimentally to increase with decreasing defect concentration.<sup>70</sup>

Turning now to the properties of magnetic solutions; the experiments of Cwik *et al.*,<sup>70</sup> reveal almost no difference in the structural properties between the magnetic

and non-magnetic solutions close to the transition temperature. Based on that, we assume that the calculated structure in the magnetic state do not differ much from the non magnetic one near the transition temperature leading to  $\Delta_{CF}^{nonmagn} = \Delta_{CF}^{magn}$ . Thus, the total splitting of the  $t_{2g}$  states in a magnetic state ( $\Delta_{tot}^{magn}$ ) is a result of the interplay between  $\Delta_{CF}^{nonmagn}$  due to the structural  $\text{GdFeO}_3$  distortion and spin superexchange splitting ( $\Delta_{SE}$ ).

The non-magnetic minimum was used for subsequent *unrestricted* spin calculations where spin flips were carried out to simulate, using the same parameters, the ferromagnetic (FM) and G-type, A-type and C-type antiferromagnetic (AFM) states (see Table V and Ref. 99 for a description of the different magnetic orderings). Two reasons are beyond considering the different magnetic states: First, we want to test the ability of HSE06 to identify the ground state because previous calculation with LDA+ $U$ ,<sup>93</sup> predicted the A-type AFM state to be the ground state, which is in disagreement with the G-type AFM state found experimentally. Second, those different magnetic orders might not be observed in bulk LTO under normal conditions, but might become relevant under strain or for LTO based heterostructures. Thus, details of electronic structure of LTO in all magnetic states will be examined with focus on  $\Delta_{tot}^{magn}$ .

In the ferromagnetic and antiferromagnetic spin orientations, PBE predicts LTO as metallic, whereas experiment has shown it to be a Mott insulator.<sup>70</sup> This is a well-known limitation of semilocal functionals and agrees very well with the conclusions from early DFT studies of LTO using plane-wave basis sets.<sup>28,87,100,101</sup> This has been overcome in the past by adding the Coulomb term correction ( $U$ ) or via a GW correction.<sup>97,102</sup> HSE06 performs much better than PBE predicting the G-type AFM ordering to be the ground state and a Mott insulator.<sup>70</sup>  $\text{LaTiO}_3$  also transforms to a Mott insulator for the other magnetic orders we considered, with an energy gain relative to ground state of 21 meV for A-type AFM, 44 meV for C-type AFM and 795 meV for the FM states.

The band structure of a Mott insulator is characterized by the optical gap, which is determined by the Hubbard splitting ( $M_{gap}$ ) of the  $d$ -band separation of the lower and upper Hubbard bands; this is also called the Mott gap. The other gap is called the charge transfer gap, which is the energy difference ( $\Delta$ ) between the filled  $p$ -bands and the unoccupied upper Hubbard  $3d$ -band. For  $\text{LaTiO}_3$ , the experimental Mott gap is 0.1 eV according to the measurements of Arima *et al.*<sup>103</sup> while the CT gap is 4.5 eV.

The nature of the band gap (direct vs. indirect), the shape and the width of the Mott bands as well as the amount of  $\Delta_{tot}^{magn}$  are discussed below: In the G-type AFM (Figure 6), the gap is indirect from  $Z \rightarrow \Gamma$  and measures 1.27 eV, separating the occupied lower Hubbard band from the unoccupied higher Hubbard band, the Mott band is 1 eV, showing a  $\Delta_{tot}^{magn}$  of 700 meV. In the A-type AFM ordering we observe a larger, indirect

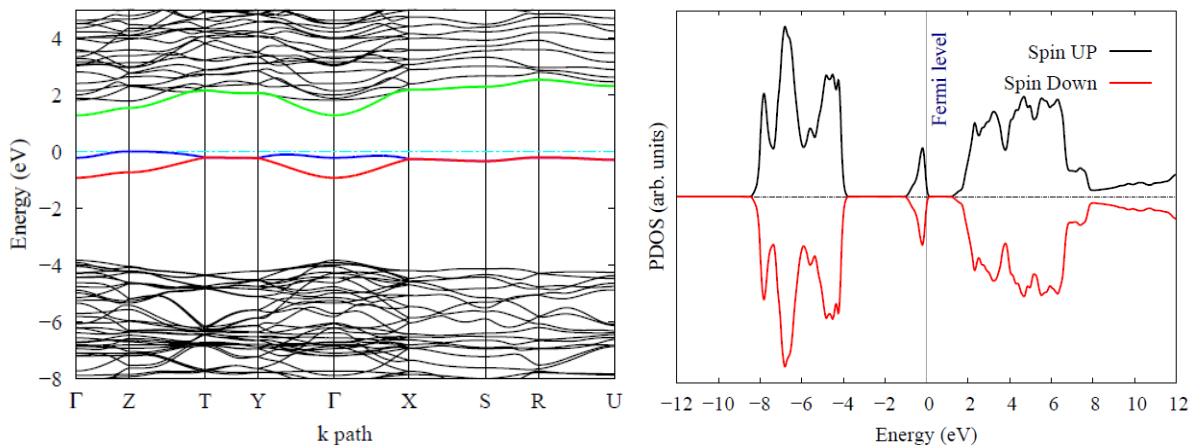


FIG. 6. (Color online) Band structure and PDOS for LaTiO<sub>3</sub> in the G-Type antiferromagnetic spin orientation. The Ti  $t_{2g}$  triplet bands can be distinguished by their colors and  $\Delta_{tot}^{magn}$  is evaluated from the separation of the two bottom ones.

TABLE V. Calculated HSE06 energy differences referenced to the G-type antiferromagnetic (AFM) ground state ( $\Delta E$ ), the Mott gap ( $M_{gap}$ ), the charge transfer gap ( $\Delta$ ) and the magnetic moments ( $\mu$ ) for the Ti atoms as obtained from the Mulliken population analysis of the spin density. The separation between the O-2p states and the first Ti-3d states ( $\Delta_{pd}$ ), the width of the Mott band ( $E_M$ ) as well as the value of the first splitting of the  $t_{2g}$  at the  $\Gamma$  point ( $\Delta_{tot}^{magn}$ ) are also reported.

	Spin	$\Delta E$ (meV)	$M_{gap}$ (eV)	$\Delta$ (eV)	$\mu$ (a.u.)	$\Delta_{pd}$ (eV)	$E_M$ (eV)	$\Delta_{tot}^{magn}$ (meV)
AFM: G-Type								
Experiment		–	0.1-0.2	4.5	0.57 <sup>a</sup> , 0.45 <sup>b</sup>	3.0 <sup>b</sup>		120-300 <sup>c</sup>
Prev. Calcs.		–	1.6 <sup>c</sup> , 0.57 <sup>d</sup>	5.2 <sup>c</sup> , 3.5 <sup>d</sup>	0.89 <sup>c</sup> , 0.78 <sup>d</sup>	3.1 <sup>c</sup> , 2.3 <sup>d</sup>		400 <sup>c</sup> , 230 <sup>d</sup>
		–	0.77 <sup>e</sup>		0.68 <sup>e</sup>			140 <sup>f</sup> , 54 <sup>g</sup>
This Work								
AFM G-Type	$\uparrow \downarrow$ $\downarrow \uparrow$	0	1.27	5.2	0.94	2.9	1.0	700
AFM A-Type	$\downarrow \downarrow$ $\uparrow \uparrow$	21	1.39	5.0	0.90	3.0	0.6	326
AFM C-Type	$\uparrow \downarrow$ $\uparrow \downarrow$	44	0.93	4.9	0.92	2.9	1.4	660
FM	$\uparrow \uparrow$ $\uparrow \uparrow$	795	1.02	5.2	0.92	2.5	1.8	720

<sup>a</sup> Ref 70

<sup>b</sup> Ref 96

<sup>c</sup> Ref<sup>92</sup>

<sup>d</sup> VPSIC results from ref 74 for non relaxed structures.

<sup>e</sup> LDA+ $U$  results form ref 93 using the experimental LaTiO<sub>3</sub> structure at 8 K from Ref 70.

<sup>f</sup> DFT+ $U$ +GWA form ref 97.

<sup>g</sup> LDA+ $U$  results form ref 98.

<sup>h</sup> LDA+ $U$  results form ref 91.

band gap from  $R \rightarrow \Gamma$  of 1.39 eV, but a narrower Mott band (sharper and thinner) due to the reduced splitting between the  $t_{2g}$  states, ca. 320 meV. In the C-type AFM spin orientation, the indirect gap from  $S \rightarrow \Gamma$  has the smallest value, 0.9 eV, but  $\Delta_{tot}^{magn}$  is comparable to the G-type ordering value while the Mott band is larger by 0.4 eV. In the FM state, we find a direct band gap of 1 eV and  $\Delta_{tot}^{magn}$  comparable to the G-type ordering value while the Mott band is larger by 0.8 eV.

Our calculated Mott gaps, CT gaps and magnetic moments for various magnetic orders are summarized in Table V and compared to experiments and previous calculations. The separation between the O-2p states and the first Ti-3d states ( $\Delta_{pd}$ ), the width of the Mott band ( $E_M$ ) as well as the value of the first splitting of the  $t_{2g}$  at the  $\Gamma$  point ( $\Delta_{tot}^{magn}$ ) are also reported. In the G-type AFM ground state, our HSE06 value for  $\Delta_{pd}=2.9$  eV is in excellent agreement with the 3 eV

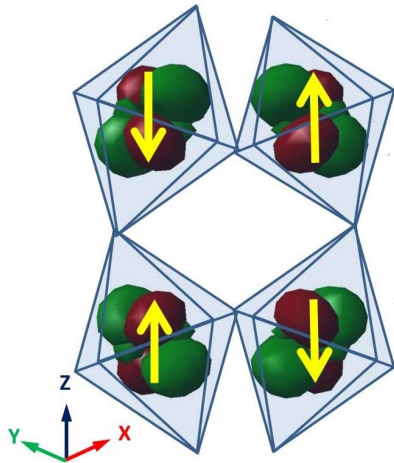


FIG. 7. (Color online) Isosurface of the highest occupied  $t_{2g}$  state orbitals for G-type AFM  $\text{LaTiO}_3$  at the  $\Gamma$  special k point. Orbitals show a ferro-orbital ordering alternating between  $d_{xz}$  and  $d_{yz}$  orientations between each neighboring  $\text{TiO}_6$  octahedra. Arrows indicate the antiferromagnetic spin orientation on Ti sublattice.

value reported experimentally.<sup>96</sup> Also, the CT gap is only 0.5 eV higher than the experimentally measured value of 4.5 eV, which constitutes an improvement over the previous LDA+ $U$  calculation.<sup>93</sup> However,  $M_{gap}$  and  $\mu$  are higher than the experimentally reported values. This overestimation obtained with HSE06 was addressed in the recent study of Rivero *et al.*,<sup>23</sup> which demonstrated that screened hybrids do provide a good *quantitative* description of the electronic structure of strongly-correlated systems, but that the magnetic coupling constants remain overestimated<sup>104–106</sup> compared to experiment. This phenomenon is observed using other theoretical methods,<sup>74,87,91,93,97,98</sup> summarized in Table V and several explanations for this wide-spread divergence of theory and experiment have been proposed.<sup>74,90</sup> It is very likely that the experimental samples are not pristine and contain defects which “metallize” them, yielding smaller gaps.

Based on our HSE06 large  $\Delta_{CF}$  and  $\mu$  values, LTO is expected to display an induced orbital order (IOO). Indeed, orbital ordering in G-type AFM  $\text{LaTiO}_3$  can be

clearly seen in Figure 7 showing the highest occupied  $t_{2g}$  state orbitals for G-type AFM  $\text{LaTiO}_3$  at the  $\Gamma$  special k point. Orbitals show a ferro-orbital ordering oriented parallel to the  $z$ -axis and oriented along the long  $\text{Ti-O}_2$  bonds. Because the *long*  $\text{Ti-O}_2$  bonds (see Figure 4-c) are perpendicular between each neighboring  $\text{TiO}_6$  octahedra, the orbitals sitting along those bonds appear alternating between  $d_{xz}$  and  $d_{yz}$  and tilted due to the  $\text{GdFeO}_3$  distortion. This picture confirm once again experiments<sup>92</sup> and theoretical calculations<sup>90</sup> suggesting that  $\text{LaTiO}_3$  has an induced orbital order and might not be an orbital liquid.

#### IV. CONCLUSIONS

The performance of the screened hybrid HSE06 was tested for modeling the fully relaxed semi-conducting metal oxide perovskites  $\text{SrTiO}_3$  and  $\text{LaAlO}_3$  in their different structural phases, and the strongly-correlated Mott insulator  $\text{LaTiO}_3$  in the ferromagnetic and various antiferromagnetic orderings. HSE06 gives good band gaps and accurate structural/geometric properties. It demonstrated great efficiency in handling structural phase transitions, and yielded accurate structural properties and order parameters (octahedral rotations/tilts and strains) for all three perovskites. This is a substantial improvement over DFT+ $U$  – one that suggests that HSE06 may be as successful in treating other metal oxides and the metal-insulator transition in oxide superlattices. In addition, the crystal field splitting ( $\Delta_{CF}$ ) of the  $t_{2g}$  states resulting from the phase transitions in  $\text{SrTiO}_3$ ,  $\text{LaAlO}_3$  and  $\text{LaTiO}_3$  was evaluated for all three materials, and showed excellent agreement with experiment in the STO case.<sup>63</sup> The LTO computed  $\Delta_{CF} = 410$  meV is rather high and indicate that  $\text{LaTiO}_3$  has an induced orbital order that shows clearly from our analysis of highest occupied  $t_{2g}$  state orbitals.

#### ACKNOWLEDGMENTS

This work is supported by the Qatar National Research Fund (QNRF) through the National Priorities Research Program (NPRP 08 - 431 - 1 - 076). We are grateful to the Research computing facilities at Texas A&M University at Qatar for generous allocations of computer resources.

\* fadwa.el\_mellouhi@qatar.tamu.edu

† ed.brothers@qatar.tamu.edu

<sup>1</sup> J. Chakhalian, A. J. Millis, and J. Rondinelli, *Nat. Mater.* **11**, 92 (2012).

<sup>2</sup> H. Y. Hwang, Y. Iwasa, M. Kawasaki, B. Keimer, N. Nagaoosa, and Y. Tokura, *Nat. Mater.* **11**, 103 (2012).

<sup>3</sup> R. Pentcheva and W. E. Pickett, *J. Phys.: Condens. Matter* **22**, 043001/1 (2010).

<sup>4</sup> P. Zubko, S. Gariglio, M. Gabay, P. Ghosez, and J.-M. Triscone, *Annu. Rev. Condens. Matter Phys.* **2**, 141 (2011).

<sup>5</sup> G. Kotliar, S. Y. Savrasov, K. Haule, V. S. Oudovenko, O. Parcollet, and C. A. Marianetti, *Rev. Modern Phys.* **78**, 865 (2006).

<sup>6</sup> K. Held, I. A. Nekrasov, G. Keller, V. Eyert, N. Blmer, A. K. McMahan, R. T. Scalettar, T. Pruschke, V. I. Anisimov, and D. Vollhardt, *Phys. Status Solidi B* **243**, 2599

- (2006).
- <sup>7</sup> D. Vollhardt, *Annalen der Physik* **524**, 1 (2012).
  - <sup>8</sup> G. Onida, L. Reining, and A. Rubio, *Rev. Modern Phys.* **74**, 601 (2002).
  - <sup>9</sup> G. Trimarchi, H. Peng, J. Im, A. J. Freeman, V. Cloet, A. Raw, K. R. Poepplmeier, K. Biswas, S. Lany, and A. Zunger, *Phys. Rev. B* **84**, 165116 (2011).
  - <sup>10</sup> A. Franceschetti and A. Zunger, *Nature* **402**, 60 (1999), 10.1038/46995.
  - <sup>11</sup> J. M. Rondinelli and N. A. Spaldin, *Phys. Rev. B* **82**, 113402 (2010).
  - <sup>12</sup> N. A. Benedek and C. J. Fennie, *ArXiv e-prints* (2011), [arXiv:1108.2915 \[cond-mat.mtrl-sci\]](https://arxiv.org/abs/1108.2915).
  - <sup>13</sup> S. S. A. Seo, M. J. Han, G. W. J. Hassink, W. S. Choi, S. J. Moon, J. S. Kim, T. Susaki, Y. S. Lee, J. Yu, C. Bernhard, H. Y. Hwang, G. Rijnders, D. H. A. Blank, B. Keimer, and T. W. Noh, *Phys. Rev. Lett.* **104**, 036401 (2010).
  - <sup>14</sup> P. Aguado-Puente, P. García-Fernández, and J. Junquera, *Phys. Rev. Lett.* **107**, 217601 (2011).
  - <sup>15</sup> B. Jalan, S. J. Allen, G. E. Beltz, P. Moetakef, and S. Stemmer, *Appl. Phys. Lett.* **98**, 132102/1 (2011).
  - <sup>16</sup> A. Janotti, D. Steiauf, and C. G. Van de Walle, *Phys. Rev. B* **84**, 201304 (2011).
  - <sup>17</sup> F. El-Mellouhi, E. N. Brothers, M. J. Lucero, and G. E. Scuseria, *Phys. Rev. B* **84**, 115122 (2011).
  - <sup>18</sup> J. P. Perdew and Y. Wang, *Phys. Rev. B* **45**, 13244 (1992).
  - <sup>19</sup> J. P. Perdew, K. Burke, and M. Ernzerhof, *Phys. Rev. Lett.* **77**, 3865 (1996).
  - <sup>20</sup> J. P. Perdew, K. Burke, and M. Ernzerhof, *Phys. Rev. Lett.* **78**, 1396 (1997).
  - <sup>21</sup> V. N. Staroverov, G. E. Scuseria, J. Tao, and J. P. Perdew, *J. Chem. Phys.* **119**, 12129 (2003).
  - <sup>22</sup> V. N. Staroverov, G. E. Scuseria, J. Tao, and J. P. Perdew, *J. Chem. Phys.* **121**, 11507 (2004).
  - <sup>23</sup> P. Rivero, I. P. R. Moreira, G. E. Scuseria, and F. Illas, *Phys. Rev. B* **79**, 245129 (2009).
  - <sup>24</sup> Z. Y. F., E. A. Kotomin, S. Piskunov, and D. E. Ellis, *Solid State Commun.* **149**, 1359 (2009).
  - <sup>25</sup> E. Heifets, E. Kotomin, and V. A. Trepakov, *J. Phys.: Condens. Matter* **18**, 4845 (2006).
  - <sup>26</sup> S. Piskunov, E. Heifets, R. I. Eglitis, and G. Borstel, *Comput. Mater. Sci.* **29**, 165 (2004).
  - <sup>27</sup> D. I. Bilc, R. Orlando, R. Shaltaf, G. M. Rignanese, J. Íñiguez, and P. Ghosez, *Phys. Rev. B* **77**, 165107 (2008).
  - <sup>28</sup> H.-S. Ahn, D. D. Cuong, J. Lee, and S. Han, *J. Korean Phys. Soc.* **49**, 1536 (2006).
  - <sup>29</sup> U. Schwingenschlögl and C. Schuster, *Chem. Phys. Lett.* **467**, 354 (2009).
  - <sup>30</sup> S. Gemming and G. Seifert, *Acta Materialia* **54**, 4299 (2006).
  - <sup>31</sup> V. Pardo and W. E. Pickett, *Phys. Rev. B* **81**, 245117 (2010).
  - <sup>32</sup> J. Lee and A. A. Demkov, *Phys. Rev. B* **78**, 193104 (2008).
  - <sup>33</sup> P. V. Ong, J. Lee, and W. E. Pickett, *Phys. Rev. B* **83**, 193106 (2011).
  - <sup>34</sup> A. D. Becke, *J. Chem. Phys.* **98**, 5648 (1993).
  - <sup>35</sup> P. J. Stephens, F. J. Devlin, C. F. Chabalowski, and M. J. Frisch, *J. Phys. Chem.*, 11623 (1994).
  - <sup>36</sup> C. Lee, W. Yang, and R. G. Parr, *Phys. Rev. B* **37**, 785 (1988).
  - <sup>37</sup> D. I. Bilc, R. Orlando, R. Shaltaf, G. M. Rignanese, J. Íñiguez, and P. Ghosez, *Phys. Rev. B* **77**, 165107 (2008).
  - <sup>38</sup> R. I. Eglitis and D. Vanderbilt, *Phys. Rev. B* **77**, 195408 (2008).
  - <sup>39</sup> J. Heyd, G. E. Scuseria, and M. Ernzerhof, *J. Chem. Phys.* **124**, 219906 (2006).
  - <sup>40</sup> J. Heyd, G. E. Scuseria, and M. Ernzerhof, *J. Chem. Phys.* **124**, 219906 (2006).
  - <sup>41</sup> T. M. Henderson, A. F. Izmaylov, G. E. Scuseria, and A. Savin, *J. Theor. Comput. Chem.* **4**, 1254 (2008).
  - <sup>42</sup> M. J. Lucero, T. M. Henderson, and G. E. Scuseria, *J. Phys. Condens. Matter* **24**, 145504 (2012).
  - <sup>43</sup> T. M. Henderson, J. Paier, and G. E. Scuseria, *Phys. Status Solidi B* **248**, 767 (2011).
  - <sup>44</sup> B. G. Janesko, T. M. Henderson, and G. E. Scuseria, *Phys. Chem. Chem. Phys.* **11**, 443 (2009).
  - <sup>45</sup> T. M. Henderson, B. G. Janesko, and G. E. Scuseria, *The Journal of Physical Chemistry A* **112**, 12530 (2008).
  - <sup>46</sup> R. Wahl, D. Vogtenhuber, and G. Kresse, *Phys. Rev. B* **78**, 104116 (2008).
  - <sup>47</sup> Y. Yamada and Y. Kanemitsu, *Phys. Rev. B* **82**, 121103 (2010).
  - <sup>48</sup> J. Paier, M. Marsman, G. Kresse, I. C. Gerber, and J. G. Ángyán, *J. Chem. Phys.* **124**, 154709 (2006).
  - <sup>49</sup> M. Marsman, J. Paier, A. Stroppa, and G. Kresse, *J. Phys.: Condens. Mat.* **20**, 064201 (2008).
  - <sup>50</sup> J. Heyd, G. E. Scuseria, and M. Ernzerhof, *J. Chem. Phys.* **118**, 8207 (2003).
  - <sup>51</sup> O. A. Vydrov and G. E. Scuseria, *J. Chem. Phys.* **125**, 234109 (2006).
  - <sup>52</sup> J. J. Phillips and J. E. Peralta, *J. Chem. Phys.* **134**, 034108 (2011).
  - <sup>53</sup> M. J. Frisch, G. W. Trucks, G. E. Schlegel, H. B. and Scuseria, M. A. Robb, J. R. Cheeseman, G. Scalmani, V. Barone, B. Mennucci, G. A. Petersson, H. Nakatsuji, M. Caricato, X. Li, H. P. Hratchian, A. F. Izmaylov, J. Bloino, G. Zheng, J. L. Sonnenberg, M. Hada, M. Ehara, K. Toyota, R. Fukuda, J. Hasegawa, M. Ishida, T. Nakajima, Y. Honda, O. Kitao, H. Nakai, T. Vreven, J. A. Montgomery, Jr., J. E. Peralta, F. Ogliaro, M. Bearpark, J. J. Heyd, E. Brothers, V. N. Kudin, K. N. and Staroverov, R. Kobayashi, J. Normand, K. Raghavachari, A. Rendell, J. C. Burant, S. S. Iyengar, J. Tomasi, M. Cossi, N. Rega, J. M. Millam, M. Klene, J. E. Knox, J. B. Cross, V. Bakken, C. Adamo, J. Jaramillo, R. Gomperts, R. E. Stratmann, O. Yazyev, A. J. Austin, R. Cammi, C. Pomelli, R. L. Ochterski, J. W. and Martin, K. Morokuma, V. G. Zakrzewski, G. A. Voth, P. Salvador, J. J. Dannenberg, S. Dapprich, A. D. Daniels, O. Farkas, J. B. Foresman, J. V. Ortiz, J. Cioslowski, and D. J. Fox, "Gaussian development version, revision h.07+,".
  - <sup>54</sup> K. N. Kudin and G. E. Scuseria, *Phys. Rev. B* **61**, 16440 (2000).
  - <sup>55</sup> ICSD, "Inorganic Crystallographic Structural Database," [www.fiz-karlsruhe.de/icsd\\_web.html](http://www.fiz-karlsruhe.de/icsd_web.html) (2010), specifically, the ICSD collection ID numbers are: STO cubic 94573, AFD 56718; LAO rhomb 92554, cubic 92561; LTO 8146, 98414, 98416 and 63573 .
  - <sup>56</sup> F. Weigend and R. Ahlrichs, *Phys. Chem. Chem. Phys.* **7**, 3297 (2005).
  - <sup>57</sup> S. H. Vosko, L. Wilk, and M. Nusair, *Can. J. Phys* **58**, 1200 (1980).
  - <sup>58</sup> CCDC 900592 - 900596 contains the supplementary crystallographic data for this paper. These data can be obtained free of charge from The Cambridge Crystal-

- lographic Data Centre via [www.ccdc.cam.ac.uk/data\\_request/cif](http://www.ccdc.cam.ac.uk/data_request/cif).
- <sup>59</sup> H. Unoki and T. Sakudo, *J. Phys. Soc. Jpn.* **23**, 546 (1967).
- <sup>60</sup> A. Heidemann and H. Wettengel, *Z. Phys.* **258**, 429 (1973).
- <sup>61</sup> R. Bistritzer, G. Khalsa, and A. H. MacDonald, *Phys. Rev. B* **83**, 115114/1 (2011).
- <sup>62</sup> Y. J. Chang, A. Bostwick, Y. S. Kim, K. Horn, and E. Rotenberg, *Phys. Rev. B* **81**, 235109 (2010).
- <sup>63</sup> H. Uwe, R. Yoshizaki, T. Sakudo, A. Izumi, and T. Uzumaki, *Jpn. J. Appl. Phys., Part 1* **24**, 335 (1985).
- <sup>64</sup> L. F. Mattheiss, *Phys. Rev. B* **6**, 4740 (1972).
- <sup>65</sup> Z. Q. Liu, D. P. Leusink, X. Wang, W. M. Lü, K. Gopinadhan, A. Annadi, Y. L. Zhao, X. H. Huang, S. W. Zeng, Z. Huang, A. Srivastava, S. Dhar, T. Venkatesan, and Ariando, *Phys. Rev. Lett.* **107**, 146802 (2011).
- <sup>66</sup> C. J. Howard, B. J. Kennedy, and B. C. Chakoumakos, *J. Phys.: Condens. Matter* **12**, 349 (2000).
- <sup>67</sup> S. A. Hayward, F. D. Morrison, S. A. T. Redfern, E. K. H. Salje, J. F. Scott, K. S. Knight, S. Tarantino, A. M. Glazer, V. Shuvaeva, P. Daniel, M. Zhang, and M. A. Carpenter, *Phys. Rev. B* **72**, 054110 (2005).
- <sup>68</sup> H. Lehnert, H. Boysen, J. Schneider, F. Frey, D. Hohlwein, P. Radaelli, and H. Ehrenberg, *Z. Kristallogr.* **215**, 536 (2000).
- <sup>69</sup> P. Mori-Sánchez, A. J. Cohen, and W. Yang, *Phys. Rev. Lett.* **100**, 146401 (2008).
- <sup>70</sup> M. Cwik, T. Lorenz, J. Baier, R. Müller, G. André, F. Bourée, F. Lichtenberg, A. Freimuth, R. Schmitz, E. Müller-Hartmann, and M. Braden, *Phys. Rev. B* **68**, 060401 (2003).
- <sup>71</sup> A. A. Knizhnik, I. M. Iskandarova, A. A. Bagaturyants, B. V. Potapkin, L. R. C. Fonseca, and A. Korkin, *Phys. Rev. B* **72**, 235329 (2005).
- <sup>72</sup> X. Luo and B. Wang, *J. Appl. Phys.* **104**, 053503/1 (2008).
- <sup>73</sup> H. Seo and A. A. Demkov, *Phys. Rev. B* **84**, 045440/1 (2011).
- <sup>74</sup> A. Filippetti, C. D. Pemmaraju, S. Sanvito, P. Delugas, D. Puggioni, and V. Fiorentini, *Phys. Rev. B* **84**, 195127 (2011).
- <sup>75</sup> S.-G. Lim, S. Kriventsov, T. N. Jackson, J. H. Haeni, D. G. Schlom, A. M. Balbashov, R. Uecker, P. Reiche, J. L. Freeouf, and G. Lucovsky, *J. Appl. Phys.* **91**, 4500 (2002).
- <sup>76</sup> X. Luo, B. Wang, and Y. Zheng, *Phys. Rev. B: Condens. Matter Mater. Phys.* **80**, 104115/1 (2009).
- <sup>77</sup> K. Xiong, J. Robertson, and S. J. Clark, *Microelectron. Eng.* **85**, 65 (2008).
- <sup>78</sup> Y.-i. Matsushita, K. Nakamura, and A. Oshiyama, *Phys. Rev. B* **84**, 075205 (2011).
- <sup>79</sup> J. Robertson, K. Xiong, and S. J. Clark, *Phys. Status Solidi B* **243**, 2054 (2006).
- <sup>80</sup> J. W. Reiner, A. Posadas, M. Wang, M. Sidorov, Z. Kriovakapic, F. J. Walker, T. P. Ma, and C. H. Ahn, *J. Appl. Phys.* **105**, 124501 (2009).
- <sup>81</sup> V. M. Goldsmith, *Geochemische Verteilungsgesetze der Elemente VII-VIII* (1928).
- <sup>82</sup> K. Uchida, S. Tsuneyuki, and T. Shimizu, *Phys. Rev. B* **68**, 174107 (2003).
- <sup>83</sup> M. Eitel and J. E. Greedan, *J. Less-Common Met.* **116**, 95 (1986).
- <sup>84</sup> D. A. MacLean, H.-N. Ng, and J. E. Greedan, *J. Solid State Chem.* **30**, 35 (1979).
- <sup>85</sup> C. J. Pickard, B. Winkler, R. K. Chen, M. C. Payne, M. H. Lee, J. S. Lin, J. A. White, V. Milman, and D. Vanderbilt, *Phys. Rev. Lett.* **85**, 5122 (2000).
- <sup>86</sup> I. Solovyev, N. Hamada, and K. Terakura, *Phys. Rev. B* **53**, 7158 (1996).
- <sup>87</sup> S. Okatov, A. Poteryaev, and A. Lichtenstein, *Europhys. Lett.* **70**, 499 (2005).
- <sup>88</sup> E. Pavarini, A. Yamasaki, J. Nuss, and O. K. Andersen, *New J. Phys.* **7**, No pp. given (2005).
- <sup>89</sup> S. Krivenko, [Phys. Rev. B \*\*85\*\*, 064406 \(2012\)](https://doi.org/10.1103/PhysRevB.85.064406).
- <sup>90</sup> M. Mochizuki and M. Imada, *New J. Phys.* **6**, 154 (2004).
- <sup>91</sup> I. V. Solovyev, *Phys. Rev. B* **69**, 134403 (2004).
- <sup>92</sup> M. W. Haverkort, Z. Hu, A. Tanaka, G. Ghiringhelli, H. Roth, M. Cwik, T. Lorenz, C. Schüssler-Langeheine, S. V. Streltsov, A. S. Mylnikova, V. I. Anisimov, C. de Nadai, N. B. Brookes, H. H. Hsieh, H. J. Lin, C. T. Chen, T. Mizokawa, Y. Taguchi, Y. Tokura, D. I. Khomskii, and L. H. Tjeng, *Phys. Rev. Lett.* **94**, 056401 (2005).
- <sup>93</sup> S. V. Streltsov, A. S. Mylnikova, A. O. Shorikov, Z. V. Pchelkina, D. I. Khomskii, and V. I. Anisimov, [Phys. Rev. B \*\*71\*\*, 245114 \(2005\)](https://doi.org/10.1103/PhysRevB.71.245114).
- <sup>94</sup> J.-G. Cheng, Y. Sui, J.-S. Zhou, J. B. Goodenough, and W. H. Su, [Phys. Rev. Lett. \*\*101\*\*, 087205 \(2008\)](https://doi.org/10.1103/PhysRevLett.101.087205).
- <sup>95</sup> I. V. Solovyev, *Phys. Rev. B* **74**, 054412 (2006).
- <sup>96</sup> J. P. Goral and J. E. Greedan, *J. Magn. Magn. Mater.* **37**, 315 (1983).
- <sup>97</sup> Y. Nohara, S. Yamamoto, and T. Fujiwara, *Phys. Rev. B* **79**, 195110 (2009).
- <sup>98</sup> E. Pavarini, S. Biermann, A. Poteryaev, A. I. Lichtenstein, A. Georges, and O. K. Andersen, *Phys. Rev. Lett.* **92**, 176403 (2004).
- <sup>99</sup> J. B. Goodenough, *Physical Review* **100**, 564 (1955).
- <sup>100</sup> N. Hamada, H. Sawada, I. Solovyev, and K. Terakura, *Physica B: Condensed Matter* **237-238**, 11 (1997).
- <sup>101</sup> G. Pari, S. Mathi Jaya, G. Subramoniam, and R. Asokamani, *Phys. Rev. B* **51**, 16575 (1995).
- <sup>102</sup> I. V. Solovyev, *J. Phys.: Condens. Mat.* **20**, 293201 (2008).
- <sup>103</sup> T. Arima, Y. Tokura, and J. B. Torrance, *Phys. Rev. B* **48**, 17006 (1993).
- <sup>104</sup> I. D. Prodan, G. E. Scuseria, and R. L. Martin, *Phys. Rev. B* **76**, 033101 (2007).
- <sup>105</sup> I. D. Prodan, G. E. Scuseria, and R. L. Martin, *Phys. Rev. B* **73**, 045104 (2006).
- <sup>106</sup> I. D. Prodan, J. A. Sordo, K. N. Kudin, G. E. Scuseria, and R. L. Martin, *J. Chem. Phys.* **123**, 014703 (2005).